Title: Analysis of immune signatures in longitudinal tumor samples yields insight into biomarkers of response and mechanisms of resistance to immune checkpoint blockade

Authors: Pei-Ling Chen[1,2#], Whijae Roh[1#], Alexandre Reuben[3&], Zachary A. Cooper[1,3&+], Christine N. Spencer[1], Peter A. Prieto[3], John P. Miller[1], Roland L. Bassett[4], Vancheswaran Gopalakrishnan[3], Khalida Wani[5], Mariana Petaccia De Macedo[5], Jacob L. Austin-Breneman[3], Hong Jiang[3], Qing Chang[1], Sangeetha M. Reddy[6], Wei-Shen Chen[1,2], Michael T. Tetzlaff[2], Russell J. Broaddus[2], Michael A. Davies[7], Jeffrey E. Gershenwald[3], Lauren Haydu[3], Alexander J. Lazar[2,5], Sapna P. Patel[7], Patrick Hwu[7], Wen-Jen Hwu[7], Adi Diab[7], Isabella C. Glitza[7], Scott E. Woodman[7], Luis M. Vence[8], Ignacio I. Wistuba[5], Rodabe N. Amaria[7], Lawrence N. Kwong[5], Victor Prieto[2], R. Eric Davis[9], Wencai Ma[9], Willem W. Overwijk[7], Arlene H. Sharpe[10], Jianhua Hu[4], P. Andrew Futreal[1], Jorge Blando[5], Padmanee Sharma[8,11], James P. Allison[8], Lynda Chin[1]*, & Jennifer A. Wargo[1,3]*

Affiliations:

[1]Department of Genomic Medicine, [2]Pathology, [3]Surgical Oncology, [4]Biostatistics, [5]Translational Molecular Pathology, [6]Cancer Medicine, [7]Melanoma Medical Oncology, [8]Immunology, [9]Lymphoma/Myeloma, [11]Genitourinary Medical Oncology, University of Texas MD Anderson Cancer Center; Houston, TX

[10]Department of Microbiology and Immunobiology, Harvard Medical School, Boston, MA 02115 USA

77030 USA

[#] These authors contributed equally to this work

[&] These authors contributed equally to this work

* These authors shared senior authorship of this work

[+] Currently at MedImmune, Gaithersburg, MD

Corresponding author:

Jennifer A. Wargo, MD, MMSc

Email: JWargo@mdanderson.org

Address: 1400 Pressler Street, FCT 17.6060, Unit 1484, Houston, TX 77030

Email: JWargo@mdanderson.org

Telephone: (713) 745- 1553

Running title: Immune signatures of response and resistance to checkpoint blockade

Keywords: Melanoma, Immune Checkpoint, anti-CTLA-4, anti-PD-1, CD8

Financial Support

JAW acknowledges the Melanoma Research Alliance Team Science Award, the Kenedy Memorial Foundation grant #0727030, U54CA163125, STARS award, UT Regents, and the generous philanthropic support of several families whose lives have been affected by melanoma. This work was supported by National Institutes of Health grants 1K08CA160692-01A1 (JAW), U54CA163125 (ZAC, JAW, and LC), T32CA009599 (PAP), T32CA163185 (PLC, WSC), and 2P30CA016672 (IIW). WR is supported by the CPRIT Graduate Scholar Award. ICG holds a Conquer Cancer Foundation ASCO Young Investigator Award. LC is a CPRIT Scholar in Cancer Research and was supported by a grant from the Cancer Prevention Research Institute of Texas (R1204). PAF holds CPRIT funding (R1205 01),a Robert Welch Distinguished University Chair (G-0040) and STARS award. RNA has received research support from Merck, Novartis/Array and Bristol-Myers Squibb. WJH has received research support from Bristol-Myers Squibb, Merck, GSK and MedImmune. IIW has received support from the

MD Anderson's Institutional Tissue Bank. This work was supported by MD Anderson's Institutional Tissue Bank Award (2P30CA016672) from the National Cancer Institute. This study was also supported by philanthropic contributions to The University of Texas MD Anderson Cancer Center Melanoma Moon Shot Program.

Competing financial interests

J.A. Wargo has honoraria from speakers' bureau of Dava Oncology, Illumina and is an advisory board member for GlaxoSmithKline,Roche/Genentech, Novartis, and Bristol-Myers Squibb. M.A. Davies is an advisory board member for GlaxoSmithKline, Roche/Genentech, Novartis and Sanofi-Aventis and has received research support from GlaxoSmithKline, Roche/Genentech, Sanofi-Aventis, Oncothyreon, Myriad, and AstraZeneca. J.E. Gershenwald is on the advisory board of Merck, and receives royalties from Mercator Therapeutics. S.P. Patel has honoraria from speakers' bureau of Dava Oncology and Merck and is an advisory board member for Amgen and Roche/Genentech. P. Hwu serves on the advisory board of Lion Biotechnologies and Immatics US. R.N. WJ Hwu serves on the advisory board of Merck's melanoma advisory board. Amaria has received research support from Merck, Novartis and Bristol-Myers Squibb. W.W. Overwijk is an advisory board member for Immatics GmbH and 7 Hills Pharmaceuticals and has received research support from Immatics GmbH, 7 Hills Pharmaceuticals, Verastem, Memgen and Nektar Therapeutics. I.I. Wistuba receives honoraria from Genentech/Roche, Ventana, GlaxoSmithKline, Celgene, Bristol-Myers Squibb, Synta Pharmaceuticals, Boehringer Ingelheim, Medscape, Clovis, AstraZeneca and Pfizer, and research support from Genentech/Roche, Oncoplex, and HGT. P. Sharma is a consultant for Bristol-Myers Squibb, Jounce Therapeutics, Helsinn, and GlaxoSmithKline as well as a stockholder from Jounce Therapeutics. J.P. Allison is a consultant and stockholder for Jounce Therapeutics, receives royalties from Bristol-Myers Squibb, and has intellectual property with Bristol-Myers Squibb and Merck. A. H. Sharpe has patents/pending royalties on the PD-1 pathway from Roche and Novartis. A.H.S. is a consultant for Novartis, has served on advisory boards for CoStim and Bristol-Myers-Squibb, and is presently on the scientific advisory boards of Surface Oncology and SQZ Biotech, and receives research grants from Novartis and Roche. ZAC is an employee in MedImmune and owns stock or options in AstraZeneca. No other potential conflicts of interest were disclosed.

Word Count: 3501 words

Total # of Figures: 4

Total # of Tables: 0

Abstract

Immune checkpoint blockade represents a major breakthrough in cancer therapy, however responses are not universal. Genomic and immune features in pre-treatment tumor biopsies have been reported to correlate with response in patients with melanoma and other cancers, but robust biomarkers have not been identified. We studied a cohort of metastatic melanoma patients initially treated with cytotoxic T-lymphocyte-associated antigen-4 (CTLA-4) blockade (n=53) followed by programmed death-1 (PD-1) blockade at progression (n=46), and analyzed immune signatures in longitudinal tissue samples collected at multiple time points during therapy. In these studies, we demonstrate that adaptive immune signatures in tumor biopsy samples obtained early during the course of treatment are highly predictive of response to immune checkpoint blockade, and also demonstrate differential effects on the tumor microenvironment induced by CTLA-4 and PD-1 blockade. Importantly, potential mechanisms of therapeutic resistance to immune checkpoint blockade were also identified.

Significance:

These studies demonstrate that adaptive immune signatures in early on-treatment tumor biopsies are predictive of response to checkpoint blockade, and yield insight into mechanisms of therapeutic resistance. These concepts have far-reaching implications in this age of precision medicine, and should be explored in immune checkpoint blockade treatment across cancer types.

Introduction:

Major advances have been made in the treatment of metastatic melanoma through the use of immune checkpoint blockade, with the FDA approval of numerous therapeutic regimens within the past several years (1-6) and many more being studied in clinical trials (7, 8). Treatment with immune checkpoint inhibitor monotherapy (such as monoclonal antibodies targeting CTLA-4 and PD-1) is associated with response rates of 8-44%, and many of these responses are durable (i.e., >2 years).

However the majority of patients do not respond to these regimens as monotherapy, and some patients develop significant toxicity (2, 9-11), particularly when these regimens are combined (4). Given these complexities, a critical need exists to identify biomarkers that accurately predict which patients will benefit from this form of therapy.

While several genomic and immune predictors of response have been reported based on analysis of pre-treatment tumor biopsies, these biomarkers are not very robust, and there is significant overlap between responders and non-responders to therapy for the markers tested (12-15). Genomic and RNA-based studies exploring predictors of outcome to immune checkpoint blockade in melanoma suggest that tumor-specific mutational load and neoantigen signature as well as cytolytic activity are significantly associated with clinical benefit and increased overall survival (13, 16, 17). Immunohistochemistry-based studies also support the notion that $CD8^+$, $CD4^+$, PD-1^+ and PD-$L1^+$ cell densities in pre-treatment biopsies can predict response to therapy (14, 15). However, cumulative evidence from these studies suggests that these biomarkers are not perfectly predictive (13, 14), and better biomarkers are clearly needed to optimize therapeutic decisions.

In addition to identifying predictors of response to immune checkpoint blockade, there is growing interest in understanding the mechanistic differences between different forms of immune checkpoint blockade. Transcriptome and pathway analysis using purified human T cells and monocytes from patients on either CTLA-4 or PD-1 blockade demonstrates distinct gene expression profile and immunologic effects between these forms of therapy (18, 19). Whereas CTLA-4 blockade induces a proliferative signature in memory T cells, PD-1 blockade leads to changes in genes implicated in cytolysis and NK cell function (19). This notion is further supported by animal models that demonstrate differential effects of CTLA-4 and PD-1 blockade therapies on the transcriptional profiles of tumor-infiltrating CD8+ T cells, with increased NFAT-JAK-STAT signaling, cell proliferation/cell cycle, and

activation of effector T cell pathways seen in CTLA-4 blockade versus changes in IL-2 signaling, response to type I IFN, and metabolic pathways seen in PD-1 blockade (18).

Along with this, there is a critical need to identify mechanisms of therapeutic resistance to immune checkpoint inhibitors that are potentially actionable. Groups have begun to study this (17, 20), and there is evidence that somatic mutations in antigen processing and presentation as well as up-regulation of genes involved in cell adhesion, angiogenesis, and extracellular matrix remodeling may contribute to immune escape in cancer (21). In addition, molecular analyses of human melanoma samples and animal models also suggest tumor-intrinsic oncogenic signals related to the WNT/β-catenin signaling pathway may mediate cancer immune evasion and resistance to immunotherapy – including CTLA-4 and PD-1 based therapy (22).

In this study, we sought to address each of these areas of critical need by studying a unique cohort of patients with metastatic melanoma who were initially treated with CTLA-4 blockade and were then treated with PD-1 blockade at time of progression. A deep immune analysis of longitudinal tumor samples was performed, yielding insights into biomarkers of response, mechanistic differences between each of these forms of therapy, and means of therapeutic resistance to immune checkpoint blockade.

Results

Patient cohort, checkpoint blockade treatment, and longitudinal tumor biopsies

To explore differential changes in the tumor microenvironment in distinct forms of immune checkpoint blockade, we assembled a unique cohort of 53 patients with metastatic melanoma who were initially treated with CTLA-4 blockade and were then treated with PD-1 blockade if they did not respond or progressed on therapy. The scheme of treatment and longitudinal tumor sampling is shown in **Fig. 1a**. Biopsies were obtained (when available) prior to initiation of CTLA-4 blockade, on-treatment,

and after re-staging in patients who did not respond or who progressed on therapy. Clinical responders were defined by radiographic evidence of absent disease, stable disease or decreased tumor volume for >6 months. Non-responders were defined by tumor growth on serial CT scans after the initiation of treatment or any clinical benefit lasting ≤6 months (minimal benefit) (13). Non-responders to CTLA-4 blockade were then treated with PD-1 blockade therapy, and additional biopsies were obtained early during the course of therapy and late on-treatment in non-responders (or progressors) on PD-1 blockade (**Fig. 1a**). Among the patients treated with CTLA-4 blockade, 13% achieved clinical benefit while 87% did not, consistent with published response rates (1, 11). **Supplementary Table S1a** and **b** shows the clinical and demographic characteristics of the patients in this cohort. Available biopsies were subsequently processed for downstream immune profiling by immunohistochemistry and gene expression studies (**Supplementary Table S1c-d**).

Immune profiling in early on-treatment biopsies is predictive of response to CTLA-4 blockade in a unique cohort of patients treated with sequential CTLA-4 and PD-1 blockade

The profile and kinetics of immune cell infiltrates in the tumor microenvironment were first investigated via a 12-marker immunohistochemistry (IHC) panel (**Supplementary Table S2**). At the pre-treatment time point, there was no difference in any of the measured markers between responders versus non-responders to CTLA-4 blockade (**Fig. 1b-d, Supplementary Fig. S1a-i**), consistent with previous reports (23). However, analysis of early on-treatment tumor biopsies identified a significantly higher density of $CD8^+$ T cells in responders versus non-responders to CTLA-4 blockade (**Fig. 1b**, $p<0.05$). IHC for other immune and immunomodulatory markers at the on-treatment time point on CTLA-4 blockade showed no significant differences in responders versus non-responders, though a trend towards higher PD-L1 expression was observed in responders (**Fig. 1c**, **Supplementary Fig. S1**).

Representative IHC images for CD8, CD4, and PD-L1 expression in responders and non-responders to CTLA-4 blockade are shown for each time point in **Fig. 1e-f**.

In addition, to better understand the contribution of myeloid:T cell interactions to therapeutic response, we also stained sections with additional myeloid markers (**Supplementary Table S3**). Though we saw no clear quantitative differences in any of the myeloid subsets in responders versus non-responders to CTLA-4 blockade (**Supplementary Fig. S2a-h**), we observed a slightly higher proximity of CD68+ myeloid cells to CD8+ T cells in non-responders at the pre-treatment time point (**Supplementary Fig. S3a-b**, p=0.08), however this did not reach statistical significance in this small cohort.

Immune profiling in early on-treatment biopsies is highly predictive of response to PD-1 blockade.

We next used our 12-marker IHC panel to interrogate the profile and kinetics of immune cell subsets in tumor samples from patients on anti-PD-1 therapy. Forty-six patients were included that were initially treated with CTLA-4 blockade, as well as eleven additional patients who had not received prior CTLA-4 blockade to control for possible prior CTLA-4 blockade exposure effects. In these studies, we observed a modest but statistically significant difference in the density of $CD8^+$, $CD3^+$ and $CD45RO^+$ T cells in pre-treatment samples of responders compared to non-responders (**Fig. 2a-f**, **Supplementary Fig. S4a**, p=0.03, 0.03, 0.02, respectively), though the values between these two groups were largely overlapping, consistent with prior published data (23). There was also a trend towards higher pre-treatment expression of CD4 and PD-1 in responders versus non-responders, though these did not reach statistical significance (**Fig. 2a-f,** p=0.06, p=0.08, respectively).

In contrast, there was a profound and highly statistically significant difference in the expression of markers for T cell subsets - CD8 (p=0.001), CD4 (p=0.001), and CD3 (p<0.001) - and

197 immunomodulatory molecules PD-1 ($p<0.001$), PD-L1 ($p=0.007$), and LAG-3 ($p<0.0001$) in responders
198 versus non-responders to therapy in early on-treatment tumor samples, with little to no overlap between
199 groups (**Fig. 2a-f**). Of note, a significantly higher level of expression of FoxP3 ($p<0.001$) and granzyme
200 B ($p=0.02$) was observed in responders compared to non-responders to therapy, likely relating to an
201 enhanced activation status of infiltrating T cells in responding patients (**Supplementary Fig. S4a-f**).
202 Importantly, these changes were observed in responders as early as 2-3 doses following initiation of PD-
203 1 based therapy. Representative IHC images for these markers are shown in **Fig. 2g-h**. Specific analysis
204 performed on longitudinal samples also demonstrated an increase in CD8, PD-1, and PD-L1 in
205 responders compared to non-responders to PD-1 based therapy (**Supplementary Fig. S5a-f**).

206 In light of previous studies demonstrating the importance of the invasive tumor margin in
207 predicting responses to PD-1 blockade (14), we quantified CD8+ T cells density at the tumor margin in
208 41 samples with discernable tumor margins. In these studies, we did not observe significant differences
209 in CD8+ T cells at the tumor margin between responders and non-responders to PD-1 based therapy at
210 all time points examined, though sample size was admittedly limited. However, when we compared the
211 ratio of CD8+ T cells at tumor center versus the margin in early on-treatment biopsies, we observed
212 significantly higher ratios of CD8+ T cells at the tumor center versus the margin within responders
213 compared to non-responders (**Supplementary Fig. S6a-h**), suggesting possible infiltrate from margin to
214 center of the tumor in the context of therapy.

215 To augment these studies, we performed immune profiling in the separate cohort of patients who
216 received PD-1 blockade in the absence of prior CTLA-4 exposure, and observed no significant
217 differences in our prior observations when these patients were included in the analysis (**Supplementary**
218 **Fig. S7a-h, Supplementary Table S4**). As observed previously with CTLA-4 blockade, we saw no
219 clear quantitative difference in any of the myeloid subsets in responders and non-responders to PD-1

blockade (**Supplementary Fig. S8a-i**). However, we observed a significantly higher proximity of CD68+ myeloid cells to CD8+ T cells in non-responders at the pre- and on-treatment time points for patients on PD-1 blockade (**Supplementary Fig. S3**, $p<0.05$).

Gene expression profiling in longitudinal tumor biopsies is predictive of response in patients treated with sequential CTLA-4 and PD-1 blockade.

To further dissect the tumor microenvironment-mediated response and resistance to immune checkpoint blockade and to identify potential mechanisms of therapeutic resistance, we performed targeted gene expression profiling (GEP) via a custom 795 gene NanoString panel composed of immune-related genes and genes pertaining to common cancer signaling pathways (**Supplementary Table S5**) in samples with available tissue. When comparing GEP results between responders and non-responders at each individual biopsy time point, no significant differences were found at pre-treatment CTLA-4 blockade, on-treatment CTLA-4 blockade, and pre-treatment PD-1 blockade. However, early on-treatment tumor samples of patients on anti-PD-1 therapy showed 411 significantly differentially expressed genes (DEGs) in responders (FDR-adjusted $p<0.05$), mostly up-regulated as compared to non-responders (**Fig. 3a-d, Supplementary Fig. S9** and **Supplementary Table S6a-e**), including IHC markers represented in the NanoString codeset, cytolytic markers, HLA molecules, IFN-γ pathway effectors, chemokines and select adhesion molecules. Notably, a small number of DEGs (n=6) were lower in responders compared to non-responders on PD-1 blockade and included vascular endothelial growth factor (*VEGFA*), suggesting a mechanism of therapeutic resistance and a potential target for therapy, which is corroborated by data from others implicating angiogenesis in resistance to immunotherapy (24, 25)(26). Notably, though only ten of the twelve IHC markers were represented in

the NanoString codeset, all ten overlapping probes showed concordance with our IHC findings (**Supplementary Fig. S10a-j** and **S11a-j**).

We next compared gene expression profiles between pre-treatment and on-treatment time points to identify dynamic changes in the tumor microenvironment associated with each form of immune checkpoint therapy. To do this, we used the linear mixed effects model to test time trend of gene expression from pre-treatment to on-treatment and its interaction with response status for CTLA-4 and PD-1 blockade, respectively. With CTLA-4 blockade, 173 up-regulated DEGs and 101 down-regulated DEGs were identified in responders versus non-responders to therapy (**Fig. 3e**, **Supplementary Table S7)**, with up-regulated DEGs similar to those described in previously published datasets (18). With PD-1 blockade, 370 up-regulated DEGs and 6 down-regulated DEGs were identified in responders versus non-responders (**Fig. 3f, Supplementary Table S8**). Up-regulated DEGs related to processes such as antigen presentation, T cell activation and T cell homing. Importantly, we did not observe significant differences in gene expression profiles in PD-1 treated patients regardless of prior treatment with CTLA-4 blockade (**Supplementary Fig. S12, Supplementary Table S9a-c)**, however the cohort was admittedly small and we cannot exclude the possibility that these GEP may in part be due to prior treatment with CTLA-4 blockade.

To investigate mechanistic differences between the two forms of immune checkpoint blockade, we next compared the response-associated DEGs (from pre-treatment to on-treatment) in tumor biopsies of CTLA-4- versus PD-1-treated patients. In this comparison, only 117 shared DEGs were up-regulated for both CTLA-4 and PD-1 blockade (**Fig. 3g**), with 56 up-regulated DEGs unique to CTLA-4 blockade, and 253 unique to PD-1 blockade (FDR-adjusted $p<0.05$, **Supplementary Table S10**). Analysis of shared down-regulated DEGs revealed 99 which were unique to CTLA-4 blockade and 4 to PD-1 blockade (FDR-adjusted $p<0.05$, **Supplementary Table S10**), with only two common DEGs in

responders versus non-responders across both forms of therapy, including dual serine / threonine and tyrosine protein kinase (DSTYK) and S100 Calcium Binding Protein A1 (S100A1).

To complement these studies and to explore the dynamic changes in GEP between responders and non-responders over the course of checkpoint blockade therapy, we compared GEP results for paired (same-patient) biopsies taken before and after PD-1 blockade. Heat mapping of the fold-change between paired biopsies for the 37 genes most frequently up-regulated in responders and/or down-regulated in non-responders ("Up-DEGs") clustered responders separately from non-responders (**Fig. 4** and **Supplementary Table S11a-b**). Pathway analysis of Up-DEGs showed that response to PD-1 blockade involves an adaptive immune response, with increased expression of antigen presentation molecules and markers of T cell activation in responding patients. Interestingly, many Up-DEGs were actually down-regulated in on-treatment samples of non-responders compared to pre-treatment, including interferon and HLA genes.

Discussion

Immune checkpoint blockade therapies have revolutionized the treatment of advanced melanoma and other cancer types, however, only a fraction of patients benefit from these treatments as monotherapy, and robust predictors of response and mechanisms of therapeutic resistance are currently lacking. Though data suggest a correlation between clinical response, pre-existing tumor-infiltrating lymphocytes, T-cell repertoire, tumor-intrinsic mutational load and neoantigens, the demonstrated biomarker profiles between responders and non-responders are often overlapping and not very robust (9, 15).

Together, the studies presented herein build on collective efforts to identify biomarkers of response and resistance to immune checkpoint blockade (13-15), and provide novel evidence that

assessment of adaptive immune responses early in the course of therapy is highly predictive of response - with non-overlapping immune signatures in responders versus non-responders, particularly to PD-1 blockade. These data have important clinical implications, and suggest that immune signatures in tumor biopsies should be evaluated early after initiation of treatment with immune checkpoint blockade rather than in pre-treatment tumor samples – at least until better predictive markers in pre-treatment tissue and blood samples may be identified. This is highly relevant, as many clinical trials of immune checkpoint inhibitors currently mandate assessment of immune markers only in pre-treatment tumor tissue; however our findings suggest that we should reconsider this approach and assess adaptive immune responses in patients on therapy. Of note, we recognize the immune signatures observed in early on-treatment samples may simply be a consequence of the immune response to checkpoint inhibitors, and may not represent bona fide mechanisms of therapeutic response. Additional studies are needed to fully delineate whether these immune signatures are responsible for, or a product of, the underlying mechanisms underlying the response – though are admittedly out of the context of the current study. Importantly, similar observations have been made in other tumor types (27), suggesting that such an approach could be applicable to other solid tumors – though this hypothesis needs to be tested more broadly.

These data also offer mechanistic insight into response to immune checkpoint blockade, suggesting that response to PD-1 blockade is related to enhanced cytolytic activity, antigen processing, and IFN-γ pathway components (16, 17). Interestingly, *VEGFA* was decreased in responders and increased in non-responders to therapy, suggesting a mechanism of therapeutic resistance as observed by others (24-26) and a potential target for therapy. The anti-angiogenesis pathway has been shown to interact with anti-tumor immunity through multiple mechanisms. Previous studies demonstrate that increased VEGF secretion decreases T cell effector function and trafficking to tumor (28, 29), and correlates with increased PD-1 expression on CD8 T cells (25). In addition to direct effect on T cells,

VEGF also decreases the number of immature dendritic cells as well as T cell priming ability of mature dendritic cells (30), further contributing to decreased effector T cell function. Angiogenic factors have also been shown to expand T regulatory cell (31) and myeloid-derived suppressor cell populations. Based on these findings and preclinical and translational data supporting synergy between angiogenesis inhibitors and immunotherapies, multiple trials of combination therapy are underway, including bevacizumab with anti-PD-1 therapy (26). Phase 1 trial data from advanced melanoma patients of bevacizumab and ipilimumab support synergy with this combination therapy, showing a 67% disease control rate, increased CD8 T cell tumor infiltration, and circulating memory CD4 and CD8 T cells with combination therapy (26, 32). Our data are in line with these studies and reinforce the value in these combination anti-VEGF/anti-PD-1 clinical trials.

In addition, these data provide strong evidence regarding differential effects of distinct forms of immune checkpoint blockade on the tumor microenvironment, with insight into distinct mechanisms of response and of therapeutic resistance, which is in line with prior published reports in mouse (18) and in man (19). These differences have important clinical implications, and may help guide rational therapeutic combinations of distinct immune checkpoint inhibitors and immunomodulatory agents depending on the desired treatment effect.

Finally, these studies offer novel insight into mechanisms of therapeutic resistance to immune checkpoint blockade which may be potentially actionable. Examples highlighted by these data include an angiogenic phenotype in non-responding lesions (24, 33), as well as down-regulation of antigen processing and presentation (including HLA) (34, 35), and defects in interferon signaling pathways (36). These data are also supported by the recent TCGA study demonstrating enrichment of mutations in antigen presentation machinery (including HLA and β2-m) as well as extrinsic apoptotic genes in

preventing cytotoxic cells from killing tumor cells (21). Importantly, many of these mechanisms may be targetable and could help overcome therapeutic resistance to immune checkpoint blockade.

Despite these provocative results, several limitations exist with these studies. Our sample size in the current study is admittedly limited, however similar findings have been observed in other histologies (27), and efforts to expand this cohort are currently ongoing. In addition and potentially related to the limited sample size, robust biomarkers were not identified in pre-treatment samples, which is in contrast to other published reports (14). However, this disparity could also be related to different antibodies used for the markers in question (namely PD-L1).

An important consideration is that the differences in immune infiltrates observed in responders versus non-responders to PD-1 based therapy could be related to prior treatment with CTLA-4 blockade, though gene expression analyses and immunohistochemistry results in CTLA-4 naive versus CTLA-4 experienced patients did not differ significantly. This cohort is admittedly small and results need to be validated in larger cohorts and in other histologies. Based on available data from this and other groups, biopsies should be performed early on treatment (i.e. within 2-3 cycles of therapy) to validate these studies. In addition, though these novel findings are provocative, they may be difficult to validate in other solid tumor types where acquisition of early on-treatment biopsies may be less feasible. Nonetheless, there is a critical need to study this phenomenon in other solid tumors, as results from such studies may help usher in a new paradigm for immune monitoring in the setting of immune checkpoint blockade - with emphasis placed on assessment of an adaptive immune response in an early on-treatment biopsy rather than in pre-treatment markers.

Materials and Methods

Patient Cohort

An initial cohort of 53 patients with metastatic melanoma were included in this study. These patients were treated at the UT MD Anderson Cancer Center between October 2011 and March 2015 and had tumor samples collected and analyzed under IRB-approved protocols (IRB LAB00-063; LAB03-0320; 2012-0846; PA13-0291; PA12-0305). Of note, these studies were conducted in accordance with the Declaration of Helsinki and approved by the UT MD Anderson Cancer Center institutional review board. Electronic medical charts were reviewed independently by two investigators to assign clinical response group and document other clinical parameters (**Supplementary Table S1a** and **S1b**). These 53 patients were initially treated with CTLA-4 blockade, with 7 responding, while 46 progressed. The 46 patients who progressed on CTLA-4 blockade then went on to receive PD-1 blockade therapy (Expanded Access Program for MK-3475 at the MD Anderson Cancer Center). Of these 46 patients, 13 responded to PD-1 blockade, while 33 progressed. In addition, a separate cohort of 16 CTLA-4 blockade-naïve patients were also included in this study and received PD-1 blockade only. Of these 16 patients, 12 responded, while 4 progressed. Altogether, a total of 62 patients received anti-PD-1 treatment (both CTLA-4 blockade-treated and CTLA-4 blockade-naïve), 25 responded (40%) and 37 progressed (60%). Of note, in this study, one patient received CTLA-4 blockade and progressed but did not go on to receive PD-1 blockade therapy. Clinical response (responders) was defined by radiographic evidence of freedom from disease, stable disease or decreased tumor volume for more than 6 months. Lack of a clinical response (non-responders) was defined by tumor growth on serial CT scans or a clinical benefit lasting 6 months or less (minimal benefit).

Tumor samples

Tumor samples were obtained from the MD Anderson Cancer Center Department of Pathology archive and Institutional Tumor Bank with appropriate written informed consent. Biopsy collection and analyses were approved by MD Anderson Cancer Center IRB (LAB00-063; LAB03-0320; 2012-0846; PA13-0291; PA12-0305). Tumor biopsy samples were collected at multiple time points during treatment when feasible, including pre-treatment, on-treatment and progression anti-CTLA-4 biopsies, and pre-treatment, on-treatment (dose 2-3), and progression anti-PD-1 biopsies. Biopsy sites were chosen as follows: for pre-treatment and early on-treatment biopsies, the most safely accessible tumors were biopsied; for progression biopsies, progressing tumors were sampled. The median time for pre-treatment, on-treatment and progression anti-CTLA-4 biopsies were 4.4 months prior (0 to 59.3 months, average 9.2 months), 3.2 months after (0.1 to 16.8 months, average 4.6 months), and 3.6 months after (0.2 to 38.5 months, average 8.0 months) anti-CTLA-4 treatment, respectively. The median time for pre-treatment, on-treatment and progression anti-PD-1 biopsies were 3.0 months prior (0 to 35 months, average 6 months), 1.4 months after (0.7 to 26 months, average 4.5 months), and 4.4 months after (1.6 months to 320 months, average 5 months) anti-PD-1 treatment, respectively. All specimens were excisional biopsies or surgical resection specimens. For the 16 CTLA-4 blockade-naïve patients, the median time for pre-treatment and on-treatment anti-PD-1 biopsies were 2.1 months prior and 2.8 months after, respectively, and tumor samples were excisional biopsies or surgical resection specimens.

Immune Profiling by Immunohistochemistry

Tumor samples (n=88) were formalin-fixed and paraffin-embedded, including pre-treatment anti-CTLA-4 (n=36; 5 responders and 31 non-responders), on-treatment anti-CTLA-4 (n=5; 2 responders and 3 non-responders), progression anti-CTLA-4 (n=22), pre-treatment anti-PD-1 (n=24; 7 responders and 17 non-responders), on-treatment anti-PD-1 (dose 2-3) (n=11; 5 responders and 6 non-responders), and

progression anti-PD-1 (n=12) biopsies (**Supplementary Table S1c**). To examine the effect of CTLA-4 blockade on pre- and on-treatment PD-1 blockade biopsies, additional immune profiling analysis by immunohistochemistry was performed on a separate cohort of patients treated with PD-1 blockade who were CTLA-4 blockade-naive (n=13), including pre-treatment anti-PD-1 (n=9; 7 responders and 2 non-responders) and on-treatment anti-PD-1 (n=4, 2 responders and 2 non-responders) biopsies. From each tissue block, a hematoxylin & eosin stained slide was examined to evaluate tumor cellularity. Immunohistochemistry was performed using an automated stainer (Leica Bond Max, Leica Biosystems), and the primary antibodies employed included CD3 (DAKO, A0452, 1:100), CD4 (Leica Biosystems, NCL368, 1:80), CD8 (Thermo Scientific MA5-13473, 1:25), CD20 (DAKO, L26, 1:1400), CD45RO (Leica Biosystems, PA0146, ready to use), CD57 (BD Biosciences, 347390, 1:40), CD68 (DAKO, MO876, 1:450), FoxP3 (BioLegend, 320102, 1:50), Granzyme B (Leica Microsystems, PA0291, ready to use), LAG-3 (LifeSpan Bioscience, 17B4, 1:100), PD-1 (Epitomics, ab137132, 1:250), PD-L1 (Cell Signaling Technology, 13684, 1:100), CD14 (Abcam, Ab133503, 1:100), CD33 (Leica Microsystems, LCD33-L-CE, 1:100), CD163 (Leica Biosystems, NCL-L-CD163, 1:500), and CD206 (Abcam, Ab64693, 1:2000). All slides were stained using previously optimized conditions with appropriate positive and negative controls. The IHC reaction was detected using Leica Bond Polymer Refine detection kit (Leica Biosystems) and diaminobenzidine (DAB) was used as chromogen. Counterstaining was done using hematoxylin. Immunohistochemical and hematoxylin and eosin stained slides were converted into high-resolution digital images using an Aperio slide scanner (Aperio AT Turbo, Leica Biosystems). The digital images were then analyzed using the Aperio Image Toolbox analysis software (Leica Biosystems), Aperio image analysis algorithms nuclear and cytoplasmic v9. From each e-slide, 5 x 1 mm^2 areas within the tumor region (except for small biopsy samples) were chosen by a pathologist for digital analysis. Immunohistochemical staining for CD3, CD4, CD8, CD20, CD45RO, CD57, CD68,

FoxP3, Granzyme B, LAG-3, PD-1, CD14, CD33, CD163 and CD206 was evaluated as density of cells, defined as the number of positive cells per mm^2. PD-L1 expression was evaluated in tumor cells using H-score, which includes the percentage of positive cells showing membrane staining pattern (0 to 100) multiplied by the intensity of the staining (0 to 3+), with a total score ranging from 0 to 300. The final score for each marker was expressed as the average score of the areas analyzed within the tumor region (tumor center). In addition, of the initial cohort of 88 samples scored, 41 samples showing discernable tumor margins were evaluated for CD8 density at both tumor margin and center. The final scores for each marker from each patient were then transferred to a database for statistical analysis.

Immunofluorescence

For a subset of formalin-fixed and paraffin-embedded samples (n=19), we performed immunofluorescence staining for CD8 (Thermo Scientific, MA5-13473) and CD68 (DAKO, MO876) to investigate potential myeloid:T cell interactions, including pre-treatment anti-CTLA-4 (n=5; 2 responders and 3 non-responders), on-treatment anti-CTLA-4 (n=2; 1 responder and 1 non-responder), pre-treatment anti-PD-1 (n=6; 3 responders and 3 non-responders), and on-treatment anti-PD-1 (dose 2-3) (n=6; 3 responders and 3 non-responders) biopsies. This was done following the Opal protocol staining method with CD8 in Alexa488 (1:50) and CD68 in Alexa594 (1:100).

For quantification, each individually stained DAPI, CD8, and CD68-stained section was utilized to establish the spectral library of fluorophores required for multispectral analysis. Slides were scanned using the Vectra slide scanner (PerkinElmer, Waltham, MA) under fluorescent conditions. For each marker, the mean fluorescent intensity per case was then determined as a base point from which positive calls could be established. Finally, an average of five random areas on each slide were analyzed for

contact quantification (ratio of number of CD68 cells in contact with CD8 divided by number of CD68 cells) blindly by a pathologist at 20X magnification.

NanoString Analysis

A subset of tumor samples (n=54) with adequate tissue following immune profiling were selected for NanoString analysis using a custom-designed 795 gene codeset. All tumor samples were prepared from formalin-fixed and paraffin-embedded tissue blocks, including pre-treatment anti-CTLA-4 (n=16; 5 responders and 11 non-responders), on-treatment anti-CTLA-4 (n=5; 3 responders and 2 non-responders), progression anti-CTLA-4 (n=15), pre-treatment anti-PD-1 (n=16; 7 responders and 9 non-responders), on-treatment anti-PD-1 (dose 2-3) (n=10; 5 responders and 5 non-responders), and progression anti-PD-1 (n=7) biopsies (**Supplementary Table S1d** and **S5**). Hematoxylin and eosin stained sections were prepared to evaluate tumor cellularity. Total RNA was extracted from each sample individually using RNeasy Mini Kit (QIAGEN). For each NanoString assay, 1 μg of total tissue RNA was isolated, mixed with a NanoString code set mix and incubated at 65°C overnight (16–18 hr). The reaction mixes were loaded on the NanoString nCounter Prep Station for binding and washing, and the resulting cartridge was transferred to the NanoString nCounter digital analyzer for scanning and data collection. A total of 600 fields were captured per sample to generate the raw digital counts for each sample. To examine the effect of prior CTLA-4 blockade on anti-PD1 pre-treatment and on-treatment tissue samples, a separate gene expression profiling analysis was performed using a custom-designed, 795 probe codeset on 28 samples (due to exhaustion of NanoString custom code sets used in **Fig. 3**, **4** and **Supplementary Table S9a-c**. Compared to the initial code set the β2-microglobulin probe was deleted and the Melanoma Inhibitory Activity (MIA) probe was added. The same preprocessing, normalization and statistical analysis of NanoString nCounter data were applied to these 28 anti-PD-1

samples, which included 7 pre-treatment samples (4 responders, 3 non-responders) and 8 on-treatment samples with prior CTLA-4 blockade (3 responders, 5 non-responders), as well as 8 pre-treatment samples (6 responders, 2 non-responders) and 5 on-treatment samples (2 responders and 3 non-responders) that were CTLA-4 blockade-naïve.

Statistical analysis

Immune profiling by immunohistochemistry: Analyses were performed using GraphPad Prism software (La Jolla, CA). All tests were two-sided, parametric t-tests. *P* values < 0.05 were considered statistically significant.

NanoString data preprocessing: Raw count data was preprocessed using NanoStringNorm R package *NanoStringNorm* (37). Specifically, geometric mean based scaling normalization was performed to account for technical assay variation, followed by background adjustment and RNA content normalization via annotated housekeeping genes. The most stable set of housekeeping genes (*ABCF1*, *GUSB*, *TBP*, and *TUBB*) were selected by the geNorm algorithm (38). Finally, log-2 transformed data were used for downstream analyses (**Supplementary Table S6a** and **S9c**). Unsupervised hierarchical clustering analysis, with heatmap shown in **Supplementary Fig. S13**, showed no batch effect and no significant correlations between batch, time, and clinical response.

Differential gene expression analysis: Fold change (FC) of each gene was calculated as the ratio of average gene expression intensity of the responder group to that of the non-responder group. Two-sample t-test was used to compare gene expression intensities between the responder group and the non-

responder group. To account for multiple testing, we used false discovery rate (FDR) (39), defined as the probability of being true under null hypothesis when rejected and widely used in high dimensional problems. The beta-uniform mixture (BUM) model (40) was used to obtain FDR. A gene was claimed to be differentially expressed if it showed a fold change of >2 (increased in responders) or ≤ -1/2 (increased in non-responders) and FDR≤ 0.05. Volcano plots were used to visualize $\log_2$ fold change on the x-axis and p-values on the y-axis. Each gene was color-coded based on its fold change and FDR (**Fig. 3a-d**). This analysis was performed at individual time points (pre-anti-CTLA-4, on-anti-CTLA-4, pre-anti-PD-1, and on-anti-PD-1 treatment).

Assessment of time-by-response interaction: We used a linear mixed effects model, implemented using R package *lme4*, to evaluate interactions between "Time (pre-treatment, on-treatment)" and "Response (responders, non-responder)" on gene expression intensity (41). In this model, we included Time, Response, and Time-by-Response interactions as the fixed effects and a patient-specific random intercept assumed to follow a mean-0 normal distribution. Again, FDR threshold of 0.05 was used to select genes with significant interaction between Time and Response. Genes with positive interaction coefficients showed up-regulated expression in responders or down-regulated expression in non-responders after a treatment, while genes with negative interaction coefficients showed down-regulated expression in responders or up-regulated expression in non-responders after a treatment. We used volcano plots to visualize the interaction coefficients on the x-axis and p-values on the y-axis. Each gene was color-coded based on its interaction coefficients and FDR (**Fig. 3e** and **3f)**. Such an analysis was separately performed for each treatment (anti-CTLA-4 and anti-PD-1 treatment).

NanoString paired analysis: For the analysis of paired samples, raw NanoString counts were compared between samples after anti-PD-1 therapy to those in the corresponding pre-treatment sample by Poisson distribution-based statistics as previously described (42). The 37 Up-DEGs identified by analysis of

paired samples (**Fig. 3h**), comparing expression values after anti-PD-1 therapy to the value in the pre-treatment sample, were analyzed by the hypergeometric distribution test (43) for enrichment of gene sets. Categories of gene sets came from the Molecular Signatures Database, Gene Ontology, KEGG, and a custom collection from the scientific literature (Ma_census). Gene sets with a false discovery rate q value ≤ 0.1 are displayed.

References

1. Hodi FS, O'Day SJ, McDermott DF, Weber RW, Sosman JA, Haanen JB, et al. Improved survival with ipilimumab in patients with metastatic melanoma. N Engl J Med. 2010;363:711-23.
2. Topalian SL, Hodi FS, Brahmer JR, Gettinger SN, Smith DC, McDermott DF, et al. Safety, activity, and immune correlates of anti-PD-1 antibody in cancer. N Engl J Med. 2012;366:2443-54.
3. Andtbacka RH, Kaufman HL, Collichio F, Amatruda T, Senzer N, Chesney J, et al. Talimogene Laherparepvec Improves Durable Response Rate in Patients With Advanced Melanoma. J Clin Oncol. 2015;33:2780-8.
4. Larkin J, Chiarion-Sileni V, Gonzalez R, Grob JJ, Cowey CL, Lao CD, et al. Combined Nivolumab and Ipilimumab or Monotherapy in Untreated Melanoma. N Engl J Med. 2015;373:23-34.
5. Postow MA, Chesney J, Pavlick AC, Robert C, Grossmann K, McDermott D, et al. Nivolumab and ipilimumab versus ipilimumab in untreated melanoma. N Engl J Med. 2015;372:2006-17.
6. Wolchok JD, Kluger H, Callahan MK, Postow MA, Rizvi NA, Lesokhin AM, et al. Nivolumab plus ipilimumab in advanced melanoma. N Engl J Med. 2013;369:122-33.
7. Brahmer JR, Tykodi SS, Chow LQ, Hwu WJ, Topalian SL, Hwu P, et al. Safety and activity of anti-PD-L1 antibody in patients with advanced cancer. N Engl J Med. 2012;366:2455-65.
8. Curti BD, Kovacsovics-Bankowski M, Morris N, Walker E, Chisholm L, Floyd K, et al. OX40 is a potent immune-stimulating target in late-stage cancer patients. Cancer research. 2013;73:7189-98.
9. Topalian SL, Sznol M, McDermott DF, Kluger HM, Carvajal RD, Sharfman WH, et al. Survival, durable tumor remission, and long-term safety in patients with advanced melanoma receiving nivolumab. J Clin Oncol. 2014;32:1020-30.
10. Wolchok JD, Weber JS, Maio M, Neyns B, Harmankaya K, Chin K, et al. Four-year survival rates for patients with metastatic melanoma who received ipilimumab in phase II clinical trials. Annals of oncology : official journal of the European Society for Medical Oncology / ESMO. 2013;24:2174-80.
11. Schadendorf D, Hodi FS, Robert C, Weber JS, Margolin K, Hamid O, et al. Pooled Analysis of Long-Term Survival Data From Phase II and Phase III Trials of Ipilimumab in Unresectable or Metastatic Melanoma. J Clin Oncol. 2015;33:1889-94.
12. Rizvi NA, Hellmann MD, Snyder A, Kvistborg P, Makarov V, Havel JJ, et al. Cancer immunology. Mutational landscape determines sensitivity to PD-1 blockade in non-small cell lung cancer. Science (New York, NY). 2015;348:124-8.
13. Snyder A, Makarov V, Merghoub T, Yuan J, Zaretsky JM, Desrichard A, et al. Genetic Basis for Clinical Response to CTLA-4 Blockade in Melanoma. N Engl J Med. 2014;371:2189-99.
14. Tumeh PC, Harview CL, Yearley JH, Shintaku IP, Taylor EJ, Robert L, et al. PD-1 blockade induces responses by inhibiting adaptive immune resistance. Nature. 2014;515:568-71.

15. Taube JM, Klein A, Brahmer JR, Xu H, Pan X, Kim JH, et al. Association of PD-1, PD-1 ligands, and other features of the tumor immune microenvironment with response to anti-PD-1 therapy. Clin Cancer Res. 2014;20:5064-74.
16. Van Allen EM, Miao D, Schilling B, Shukla SA, Blank C, Zimmer L, et al. Genomic correlates of response to CTLA-4 blockade in metastatic melanoma. Science (New York, NY). 2015;350:207-11.
17. Hugo W, Zaretsky JM, Sun L, Song C, Moreno BH, Hu-Lieskovan S, et al. Genomic and Transcriptomic Features of Response to Anti-PD-1 Therapy in Metastatic Melanoma. Cell. 2016;165:35-44.
18. Gubin MM, Zhang X, Schuster H, Caron E, Ward JP, Noguchi T, et al. Checkpoint blockade cancer immunotherapy targets tumour-specific mutant antigens. Nature. 2014;515:577-81.
19. Das R, Verma R, Sznol M, Boddupalli CS, Gettinger SN, Kluger H, et al. Combination therapy with anti-CTLA-4 and anti-PD-1 leads to distinct immunologic changes in vivo. Journal of immunology (Baltimore, Md : 1950). 2015;194:950-9.
20. Koyama S, Akbay EA, Li YY, Herter-Sprie GS, Buczkowski KA, Richards WG, et al. Adaptive resistance to therapeutic PD-1 blockade is associated with upregulation of alternative immune checkpoints. Nature communications. 2016;7:10501.
21. Rooney MS, Shukla SA, Wu CJ, Getz G, Hacohen N. Molecular and genetic properties of tumors associated with local immune cytolytic activity. Cell. 2015;160:48-61.
22. Spranger S, Bao R, Gajewski TF. Melanoma-intrinsic beta-catenin signalling prevents anti-tumour immunity. Nature. 2015;523:231-5.
23. Huang RR, Jalil J, Economou JS, Chmielowski B, Koya RC, Mok S, et al. CTLA4 blockade induces frequent tumor infiltration by activated lymphocytes regardless of clinical responses in humans. Clin Cancer Res. 2011;17:4101-9.
24. Ferrara N, Kerbel RS. Angiogenesis as a therapeutic target. Nature. 2005;438:967-74.
25. Voron T, Colussi O, Marcheteau E, Pernot S, Nizard M, Pointet AL, et al. VEGF-A modulates expression of inhibitory checkpoints on CD8+ T cells in tumors. J Exp Med. 2015;212:139-48.
26. Ott PA, Hodi FS, Buchbinder EI. Inhibition of Immune Checkpoints and Vascular Endothelial Growth Factor as Combination Therapy for Metastatic Melanoma: An Overview of Rationale, Preclinical Evidence, and Initial Clinical Data. Front Oncol. 2015;5:202.
27. Westin JR, Chu F, Zhang M, Fayad LE, Kwak LW, Fowler N, et al. Safety and activity of PD1 blockade by pidilizumab in combination with rituximab in patients with relapsed follicular lymphoma: a single group, open-label, phase 2 trial. The Lancet Oncology. 2014;15:69-77.
28. Motz GT, Santoro SP, Wang LP, Garrabrant T, Lastra RR, Hagemann IS, et al. Tumor endothelium FasL establishes a selective immune barrier promoting tolerance in tumors. Nat Med. 2014;20:607-15.
29. Ohm JE, Gabrilovich DI, Sempowski GD, Kisseleva E, Parman KS, Nadaf S, et al. VEGF inhibits T-cell development and may contribute to tumor-induced immune suppression. Blood. 2003;101:4878-86.
30. Gabrilovich D, Ishida T, Oyama T, Ran S, Kravtsov V, Nadaf S, et al. Vascular endothelial growth factor inhibits the development of dendritic cells and dramatically affects the differentiation of multiple hematopoietic lineages in vivo. Blood. 1998;92:4150-66.
31. Terme M, Pernot S, Marcheteau E, Sandoval F, Benhamouda N, Colussi O, et al. VEGFA-VEGFR pathway blockade inhibits tumor-induced regulatory T-cell proliferation in colorectal cancer. Cancer Res. 2013;73:539-49.
32. Hodi FS, Lawrence D, Lezcano C, Wu X, Zhou J, Sasada T, et al. Bevacizumab plus ipilimumab in patients with metastatic melanoma. Cancer immunology research. 2014;2:632-42.

33. Yuan J, Zhou J, Dong Z, Tandon S, Kuk D, Panageas KS, et al. Pretreatment serum VEGF is associated with clinical response and overall survival in advanced melanoma patients treated with ipilimumab. Cancer immunology research. 2014;2:127-32.
34. Kageshita T, Hirai S, Ono T, Hicklin DJ, Ferrone S. Down-regulation of HLA class I antigen-processing molecules in malignant melanoma: association with disease progression. Am J Pathol. 1999;154:745-54.
35. Shukla SA, Rooney MS, Rajasagi M, Tiao G, Dixon PM, Lawrence MS, et al. Comprehensive analysis of cancer-associated somatic mutations in class I HLA genes. Nature biotechnology. 2015;33:1152-8.
36. Taube JM, Anders RA, Young GD, Xu H, Sharma R, McMiller TL, et al. Colocalization of inflammatory response with B7-h1 expression in human melanocytic lesions supports an adaptive resistance mechanism of immune escape. Science translational medicine. 2012;4:127ra37.
37. Waggott D, Chu K, Yin S, Wouters BG, Liu FF, Boutros PC. NanoStringNorm: an extensible R package for the pre-processing of NanoString mRNA and miRNA data. Bioinformatics. 2012;28:1546-8.
38. Vandesompele J, De Preter K, Pattyn F, Poppe B, Van Roy N, De Paepe A, et al. Accurate normalization of real-time quantitative RT-PCR data by geometric averaging of multiple internal control genes. Genome Biol. 2002;3:Research0034.
39. Benjamini Y, Hochberg Y. Controlling the False Discovery Rate: A Practical and Powerful Approach to Multiple Testing. Journal of the Royal Statistical Society Series B (Methodological). 1995;57:289-300.
40. Pounds S, Morris SW. Estimating the occurrence of false positives and false negatives in microarray studies by approximating and partitioning the empirical distribution of p-values. Bioinformatics. 2003;19:1236-42.
41. Bates D, Maechler M, Bolker B, Walker S. Fitting Linear Mixed-Effects Models Using lme4. Journal of Statistical Software. 2015;67:1-48.
42. O'Connor CM, Sheppard S, Hartline CA, Huls H, Johnson M, Palla SL, et al. Adoptive T-cell therapy improves treatment of canine non-Hodgkin lymphoma post chemotherapy. Sci Rep. 2012;2:249.
43. Ma W, Yang D, Gu Y, Guo X, Zhao W, Guo Z. Finding disease-specific coordinated functions by multi-function genes: insight into the coordination mechanisms in diseases. Genomics. 2009;94:94-100.

Author contributions

LC and JAW shared senior authorship of this manuscript. PLC, ZAC, PAF, PS, JPA, LC and JAW supervised the project and developed concepts. PLC, ZAC, PAF, LC and JAW designed experiments. PLC, WR, ZAC, AR, MTT, AJL, JH, RLB, LNK, RED, WM, LC and JAW interpreted data. PLC, ZAC,

638 AR, CNS, PAP, VG, JLAB, WSC, SMR, MAD, JEG, AJL, SPP, PH, WJH, AD, ICG, SEW, RNA,
639 LMV, IIW, VP, RED, WM, WWO, PAF, PS, JPA, AHS, LC and JAW gave conceptual advice and
640 edited the manuscript. PLC, AR, HJ, QC, IIW, VP and JB established immunohistochemical staining
641 and imaging protocols. PLC, MTT, AJL and JB provided confirmatory pathology analyses. PLC, PAP,
642 MAD, SPP, PH, WJH, AD, ICG, SEW, RNA, LC and JAW clinically evaluated patients in the trial.
643 PLC, KW, MPDM, WSC, and JPM performed NanoString assays. WR, JH, RLB, RED and WM
644 performed statistical analysis of gene expression data. PLC, ZAC, AR, LC and JAW wrote the
645 manuscript. PLC, CNS, VG and PAP retrieved tissue and compiled clinical information and
646 demographics. MAD, SPP, PH, WJH, AD, ICG, SEW, RNA and JAW accrued patients for this study.
647
648

Figure Legends

649 **Figure 1. Immune profiling in early on-treatment biopsies is predictive of response to CTLA-4**
650 **blockade in a unique cohort of patients treated with sequential CTLA-4 and PD-1 blockade. (a)**
651 Patients with metastatic melanoma were initially treated with CTLA-4 blockade (n=53) and non-
652 responders to CTLA-4 blockade were then treated with PD-1 blockade (n=46; Expanded Access
653 Program for MK-3475 at the MD Anderson Cancer Center). Of these 46 patients, 13 responded to PD-1
654 blockade, while 33 progressed. Tumor biopsy samples were collected at multiple time points during
655 their treatment when feasible, including pre-treatment, on-treatment and progression anti-CTLA-4
656 biopsies, and pre-treatment, on-treatment (dose 2-3), and progression anti-PD-1 biopsies, for
657 downstream immune profiling by immunohistochemistry and gene expression studies. The median
658 elapsed time between tumor biopsies and treatment are shown for each time point. The profile and

kinetics of immune cell infiltrates in the tumor microenvironment were compared between responders and non-responders to CTLA-4 blockade. Tumor samples available for immune profiling by IHC included pre-treatment anti-CTLA-4 (n=36; 5 responders and 31 non-responders), on-treatment anti-CTLA-4 (n=5; 2 responders and 3 non-responders) and progression anti-CTLA-4 biopsies (n=22). **(b)** CD8 and **(c)** CD4 density, and **(d)** PD-L1 H-score in responders versus non-responders on CTLA-4 blockade are shown. Representative images at pre-treatment **(e)**, early on-treatment **(f)** time points are shown in responders versus non-responders to CTLA-4 blockade (20X magnification). Error bars represent standard error mean. *= $p \leq 0.05$, n.s.= not significant. Scale bars=200 μm.

Figure 2. Immune profiling in early on-treatment biopsies is highly predictive of response to PD-1 blockade. Longitudinal tumor biopsies were performed (at pre-treatment, early on-treatment, and late on-treatment / progression time points) in patients undergoing treatment with PD-1 blockade (n=47). The profile and kinetics of immune cell infiltrates in the tumor microenvironment were compared between responders and non-responders to PD-1 blockade. Tumor samples available for immune profiling by IHC included pre-treatment anti-PD-1 (n=24; 7 responders and 17 non-responders), on-treatment anti-PD-1 (dose 2-3) (n=11; 5 responders and 6 non-responders), and progression anti-PD-1 (n=12) biopsies (**Table S1c**). CD8 **(a),** CD4 **(b),** CD3 **(c),** PD-1 **(d),** PD-L1 (H-Score) **(e)**, and LAG-3 **(f)** density are shown in responders versus non-responders. Representative images at pre-treatment **(g)** and early on-treatment **(h)** time points are shown in responders versus non-responders to PD-1 blockade (20X magnification). Error bars represent standard error mean. *= $p \leq 0.05$, **= $p \leq 0.01$, ***= $p \leq 0.001$, n.s.= not significant. Scale bars=200 μm.

680 **Figure 3. Gene expression profiling in longitudinal tumor biopsies is predictive of response in a**
681 **unique cohort of patients treated with sequential CTLA-4 and PD-1 blockade.** Gene expression
682 profiling was performed via NanoString in longitudinal tumor biopsies from patients treated with
683 sequential CTLA-4 and PD-1 blockade (n=54), including pre-treatment anti-CTLA-4 (n=16; 5
684 responders and 11 non-responders), on-treatment anti-CTLA-4 (n=5; 3 responders and 2 non-
685 responders) and progression anti-CTLA-4 biopsies (n=15), pre-treatment anti-PD-1 (n=16; 7 responders
686 and 9 non-responders), on-treatment anti-PD-1 (dose 2-3) (n=10; 5 responders and 5 non-responders),
687 and progression anti-PD-1 (n=7) biopsies (**Supplementary Table S1d, S6a** and **S9b-c**). Volcano plots
688 illustrate the $\log_2$ fold change (FC) in gene expression (responders vs. non-responders) on the x-axis and
689 unadjusted p-values from Student's t-tests between responders and non-responders on the y-axis.
690 Differentially expressed genes (FDR-adjusted $p<0.05$ and FC >2 or $<-1/2$) between responders and non-
691 responders were highlighted in green at time of pre-treatment **(a)** and on-treatment **(b)** CTLA-4
692 blockade, pre-treatment, and **(c)** and on-treatment **(d)** PD-1 blockade. Interaction of time covariate (pre-
693 treatment, on-treatment) and response covariate (responders, non-responders) was illustrated in volcano
694 plots. Genes with significant interaction were highlighted in green (FDR-adjusted $p<0.05$ and interaction
695 >1.5 or <-1.5) for CTLA-4 blockade **(e)** and PD-1 blockade **(f)**. Venn diagram illustrates shared and
696 unique genes up- and down-modulated in CTLA-4 (red) and PD-1 (blue) blockade over treatment time
697 course **(g)**.
698
699 **Figure 4**. **Nanostring paired analysis**. For analysis of paired samples, raw NanoString counts were
700 compared between samples after anti-PD-1 therapy to those in the corresponding pre-treatment sample.
701 Shown are the 37 Up-DEGs identified by paired analysis. FDR = False-discovery rate, R = Responder,
702 NR = Non-responder.

Figure 1

Chen *et al*

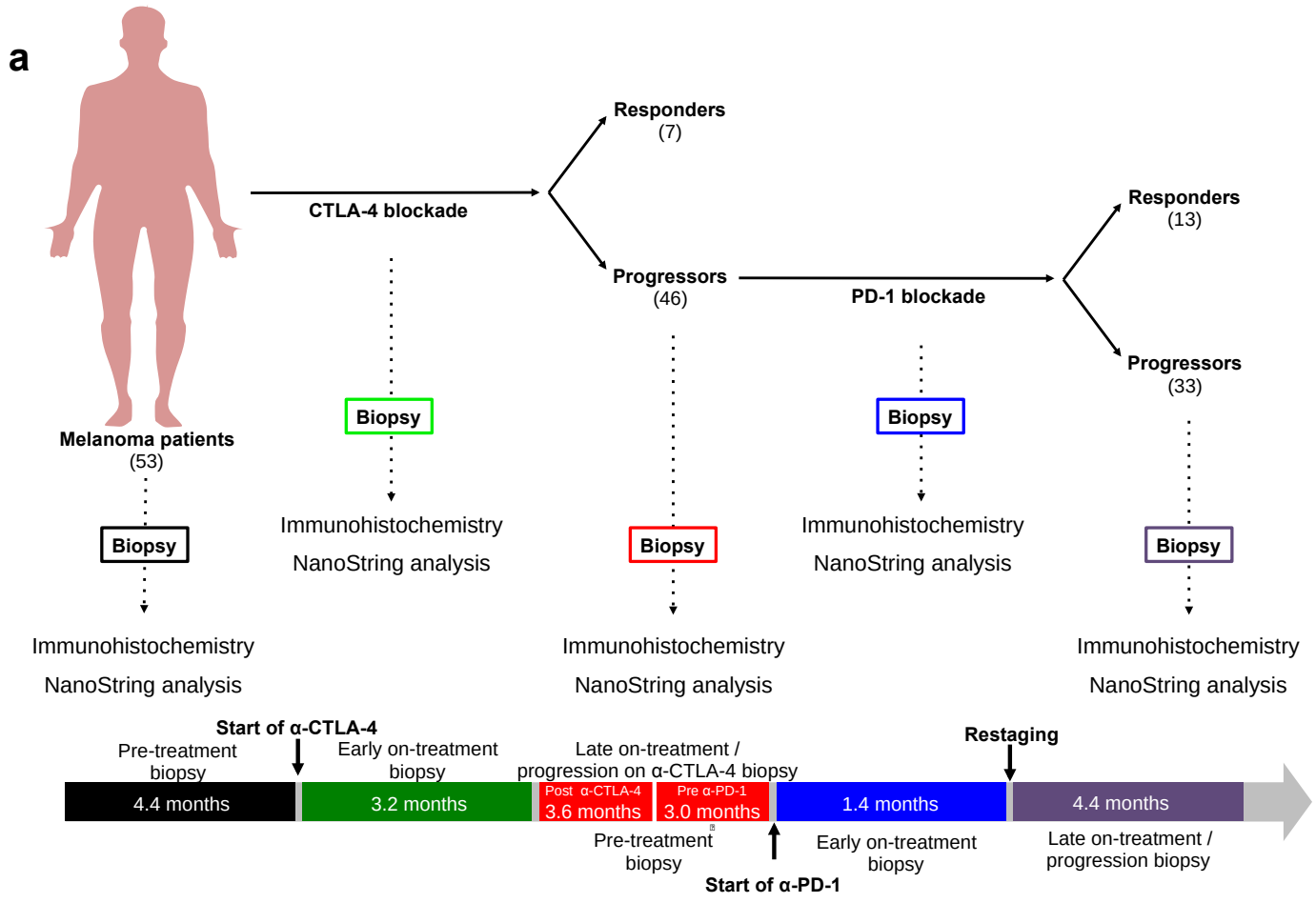

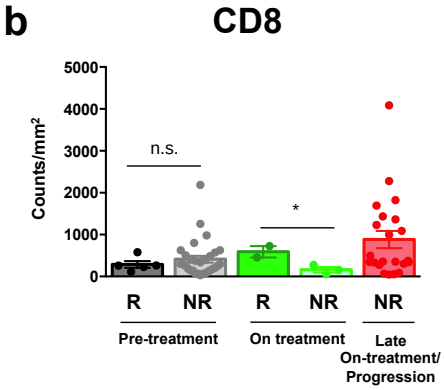

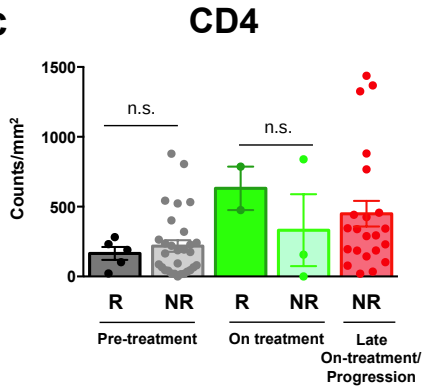

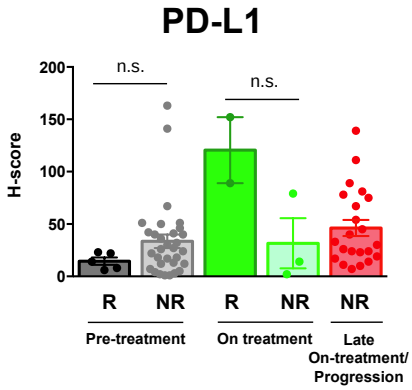

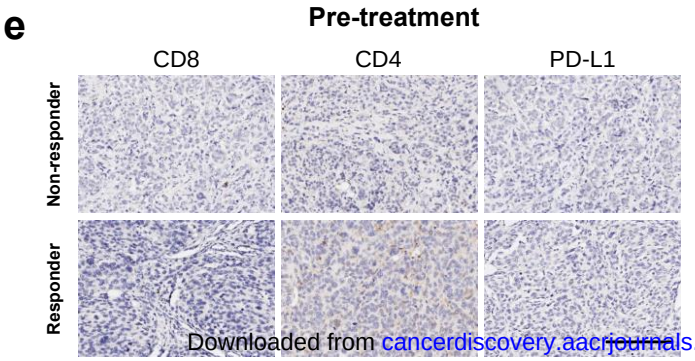

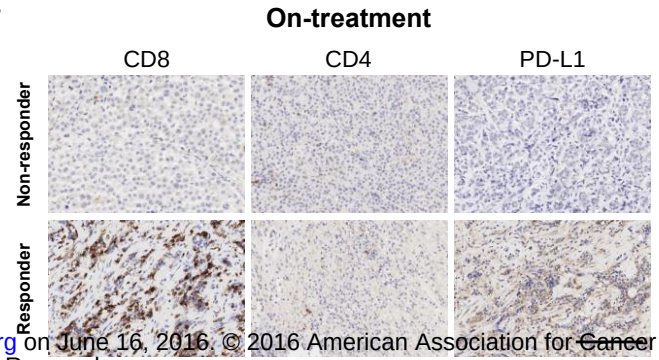

Figure 2

Chen *et al*

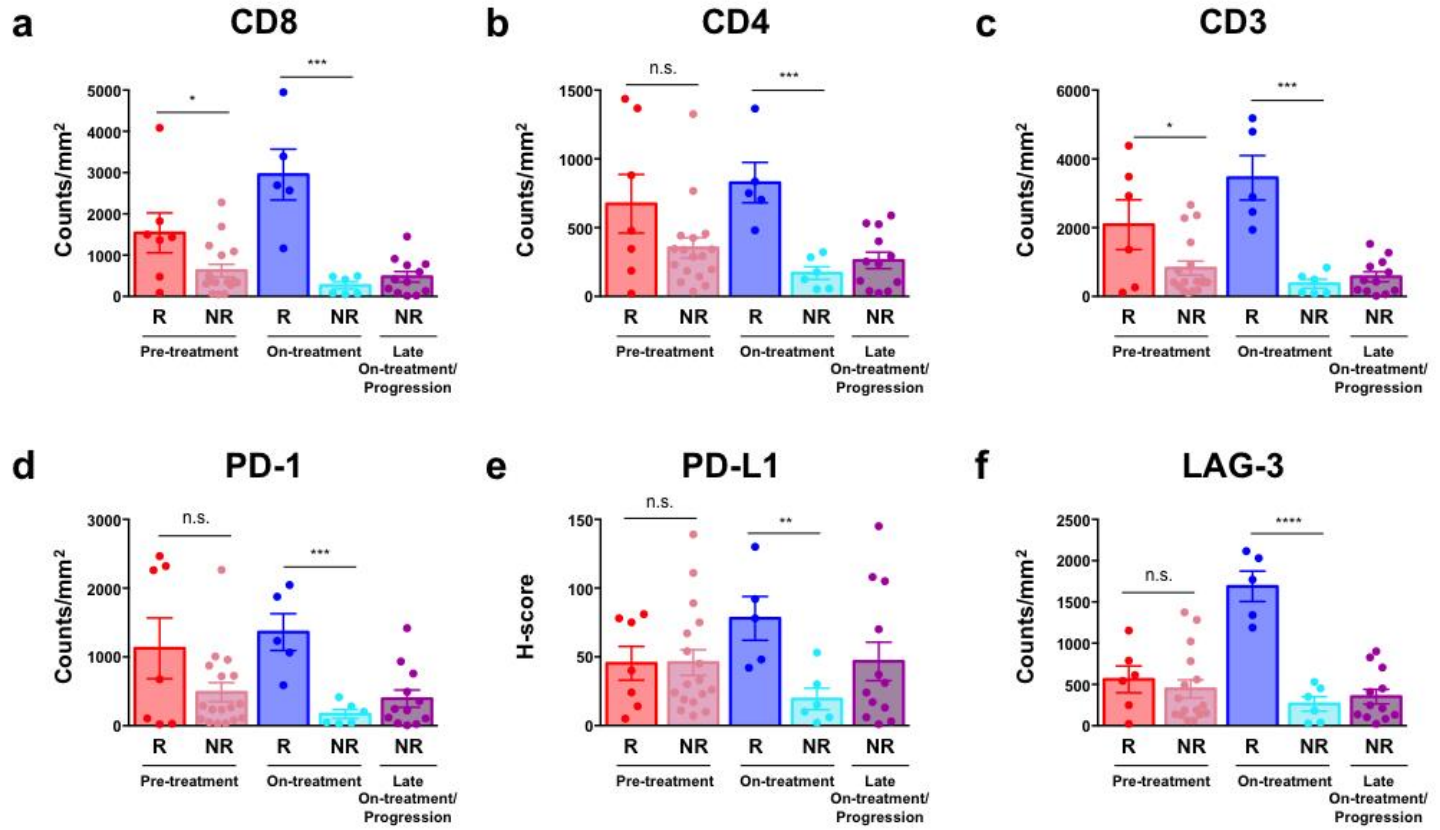

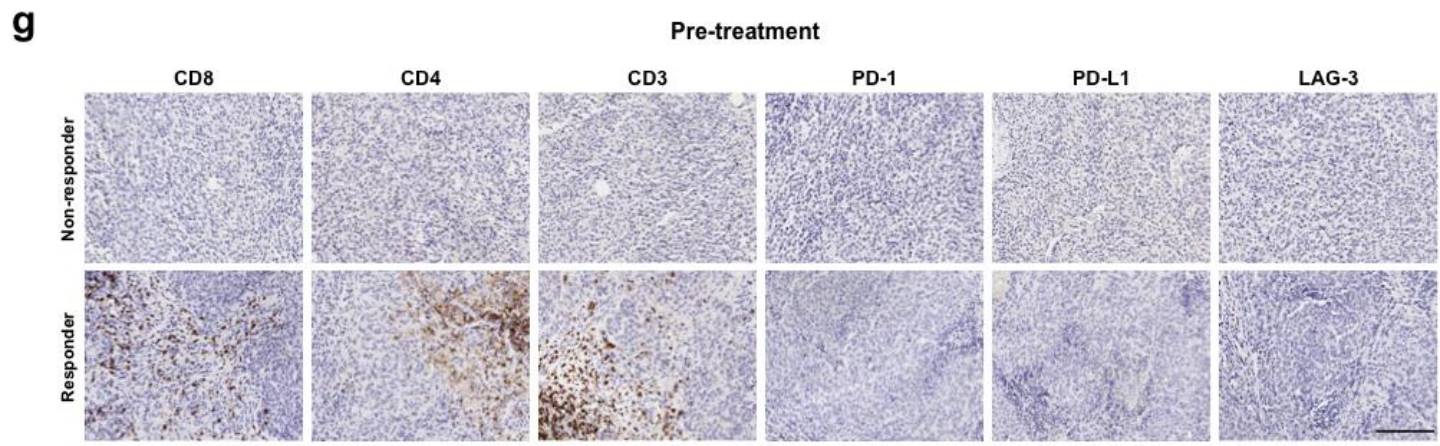

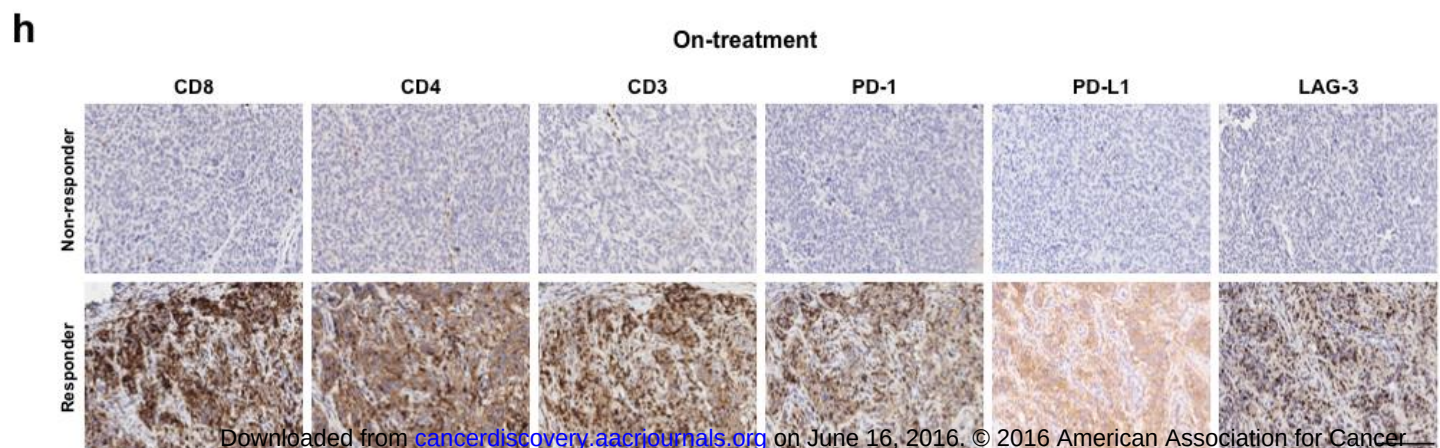

Figure 3

Chen *et al*

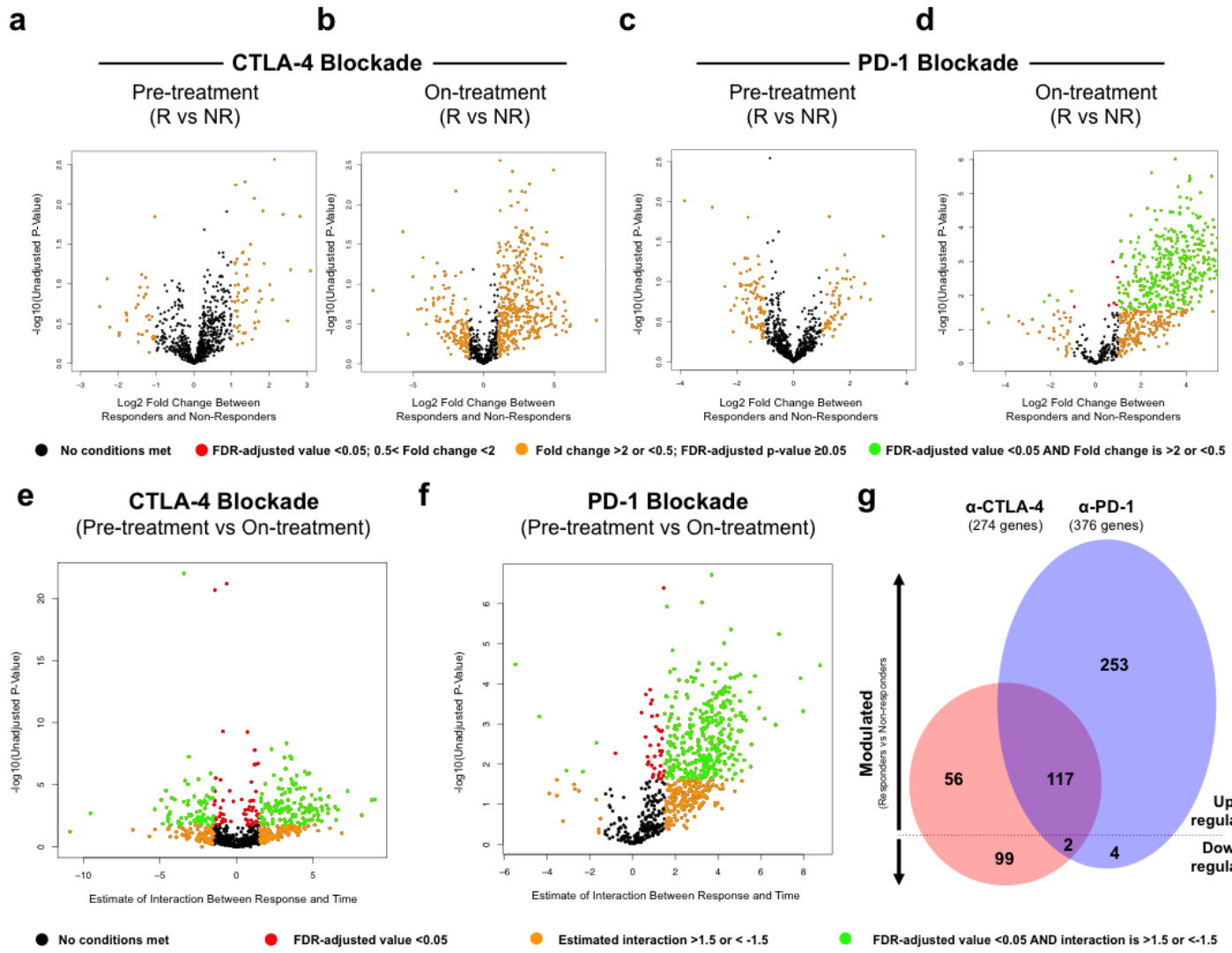

Figure 4
Chen *et al*

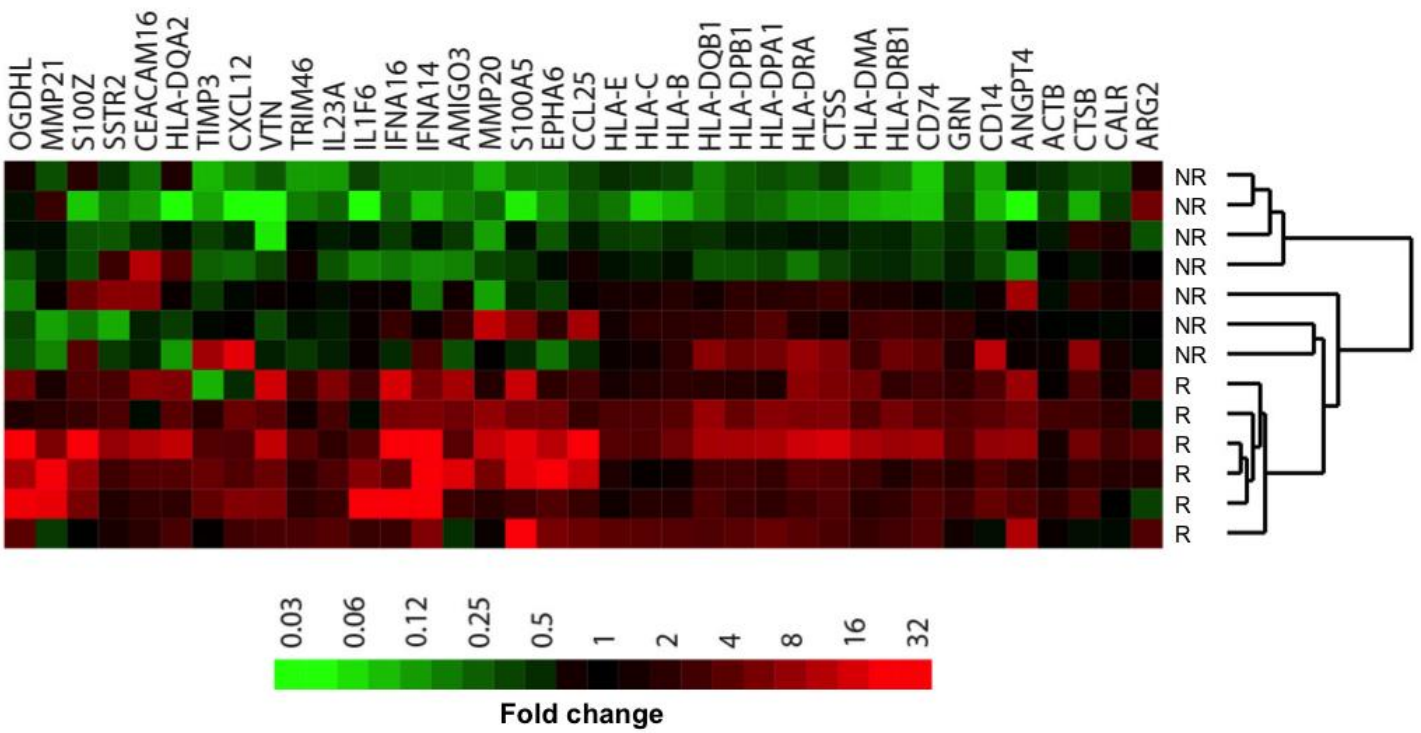

AACR American Association for Cancer Research

CANCER DISCOVERY

Analysis of immune signatures in longitudinal tumor samples yields insight into biomarkers of response and mechanisms of resistance to immune checkpoint blockade

Pei-Ling Chen, Whijae Roh, Alexandre Reuben, et al.

Cancer Discov Published OnlineFirst June 14, 2016.